2019 SECED Conference
Earthquake risk and engineering towards a resilient world
9-10 September 2019, Greenwich, London

A GROUND MOTION MODEL TO ESTIMATE NONLINEAR DEFORMATION DEMANDS FROM A RECENT PAN EUROPEAN STRONG MOTION DATABASE

Sinan Akkar[1], M. Abdullah Sandıkkaya[2]

Abstract: *Estimating nonlinear deformation demands is essential in performance based seismic design and assessment. It becomes even more important as probabilistic damage (loss) assessment becomes an important component in taking critical decisions about the resilience-based performance of structural systems. Considering these issues as the primary source of motivation, we developed two different sets of ground-motion predictive models (GMPMs) to estimate the peak single-degree-of-freedom (SDOF) inelastic deformation demands (i.e., inelastic spectral displacements). The first set of GMPMs can directly estimate the peak inelastic SDOF displacements either for constant strength (R_y) or for constant ductility (μ). The second set of inelastic GMPMs predict inelastic-to-elastic spectral displacement ratio for constant strength and constant ductility and can estimate inelastic spectra from by using the elastic displacement spectrum. The conventional source-site distance, magnitude, V_{S30} and style-of-faulting estimators in the models account for the effect of physical earthquake process on inelastic deformation demands. The second set of predictive models also account for the period-dependent correlations between elastic and inelastic spectral displacement demands for a complete conditional probabilistic representation of inelastic deformation demands. We used the proposed predictive models in probabilistic seismic hazard assessment (PSHA) to see how inelastic and elastic spectral displacement demands vary in terms of return periods. The PSHA case studies enable us to assess the design code approximation used in the estimation of nonlinear deformations from elastic spectral displacements. Our preliminary observations from the limited case studies suggest that there is still room to improve the code-based nonlinear deformation demand formulations used in simplified seismic design and assessment procedures.*

Introduction

Inelastic spectral displacement ($S_{d,ie}$) has been proposed as an important intensity measure (*IM*) for seismic performance assessment and displacement-based seismic design of structures. For example, several researchers observed a good correlation between $S_{d,ie}$ and interstory drift ratio that can be used to assess the seismic performance of structures (e.g., Miranda et al., 2004; Aslani and Miranda, 2005; Luco et al., 2003; Luco and Cornell, 2007). Inelastic spectral displacement is also a key parameter in seismic design codes to design and to verify the success of design for the target performance (e.g., TEC, 2019; ASCE, 2016).

There are several predictive models to estimate inelastic spectral displacements as a function of displacement ductility (μ; inelastic spectral displacement-to-yield displacement ratio) and strength reduction factor (R_y; elastic-to-yield strength ratio of a SDOF system). The earlier versions (e.g., Iwan, 1980; Newmark and Hall, 1982; Iwan and Guyader, 2002; Ruiz-García and Miranda, 2003; Chopra and Chintanapakdee, 2004, etc.) mostly focus on structure-significant parameters (i.e., R_y, μ or different hysteretic models) to estimate $S_{d,ie}$ for a given period. The more recent predictive models are more suitable to probabilistic structural damage and risk assessment because they treat $S_{d,ie}$ as a distribution, conditioned on R_y, μ as well as other independent ground-motion parameters such as magnitude, source-to-site distance, soil conditions and style of faulting (e.g., Tothong and Cornell, 2006; Bozorgnia et al, 2010; Stafford et al., 2016; Heresi et al., 2018).

[1] Professor, Department of Earthquake Engineering, Bogazici University 34684, Cengelkoy, Istanbul, Turkey, sinan.akkar@boun.edu.tr
[2] Assistant Professor, Department of Civil Engineering, Hacettepe University, 06800, Beytepe, Ankara, Turkey

We present two different sets of ground-motion predictive models (GMPMs) to estimate inelastic spectral displacements. The models are developed from a pan-European ground-motion database (Akkar et al., 2014a) that we used to develop several other GMPMs to estimate elastic ground-motion IMs (e.g., Akkar et al. 2014b; 2014c; Çağnan et al., 2017; Sandıkkaya and Akkar, 2017). The first set of inelastic GMPMs directly estimate 5% damped $S_{d,ie}$ for a given R_y ($S_{d,ie}^{R_y}$) or μ ($S_{d,ie}^{\mu}$). The second set of predictive models estimate the inelastic-to-elastic spectral displacement ratios for a given R_y or μ (referred to as C_R or C_μ, respectively). The estimated inelastic-to-elastic spectral displacement ratios are used with the elastic spectral displacements to predict inelastic spectral displacement either for R_y or μ. All models describe $S_{d,ie}$ as a conditional lognormal probability distribution conditioned on magnitude, soil conditions (via V_{S30}; average shear wave velocity in the upper 30 m of soil profile), source-to site distance as well as style of faulting. The paper first discusses the specific features of the proposed predictive models and displays some comparisons with similar models from the literature. This is followed by a short discussion about the implementation of the proposed predictive models in probabilistic seismic hazard assessment (PSHA) to see how different approaches to estimate $S_{d,ie}$ result in differences at specific return periods that are of significance in seismic design.

Strong-Motion Database

We extracted the ground-motion database from RESORCE (Akkar et al., 2014a); a version of the European strong-motion database with further improvements described in Sandıkkaya and Akkar (2017). This database was previously used to develop ground motion predictive models of horizontal, vertical, vertical-to-horizontal spectral acceleration ordinates as well as Arias intensity, cumulative absolute velocity and significant duration (see Akkar et al., 2014b; 2014c; Çağnan et al., 2017; Sandıkkaya and Akkar, 2017 for the above models). The database consists of 1041 three-component, free-field accelerograms recorded from 221 shallow active crustal earthquakes (Figure 1 illustrates M_w vs. R_{JB} scatter). We compute peak inelastic displacements for a 5%-damped, bilinear SDOF system having a post-yielding stiffness ratio of α = 0.03 for constant strength reduction factor (R_y; elastic-to-yield strength ratio) and for constant ductility (μ; peak inelastic-to-yield displacement ratio) for each accelerogram in the database. We consider constant strength and ductility values ranging between 1.5 and 6 (i.e., 1.5, 2, 2.5, 3, 4, 5 and 6) in the analyses to estimate the deformation demands on SDOF systems at different inelasticity levels as functions of magnitude, distance and other independent model parameters in our GMPMs. Constant strength and ductility inelastic displacement spectra serve for seismic performance assessment and design of existing and new structures. The period range we picked is between 0.05 s and 4 s, which is the same in the GMPMs developed from the same database.

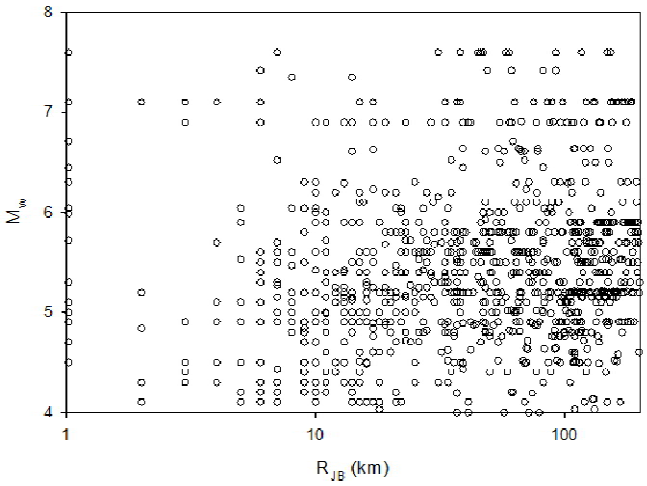

Figure 1. M_w vs. R_{JB} scatter of the ground-motion database.

Functional Form and Regressions

We developed predictive models for direct estimation of peak inelastic SDOF displacements (inelastic spectral displacements hereafter) given a constant strength or constant ductility. We also developed another set of GMPMs to estimate the ratios of inelastic-to-elastic spectral displacement for constant strength or constant ductility. One has to implement the latter models

together with elastic spectral displacement to estimate the inelastic spectra displacement. These models are rather suitable for code implementation as seismic hazard is defined in terms of elastic spectral ordinates at different return periods in seismic design codes and the engineer has to compute the peak nonlinear structural deformations from the designated elastic ground-motion hazard.

We used the same functional forms of Akkar et al. (ASB14; 2014a) for the inelastic GMPMs but we disregarded the soil nonlinearity for simplicity. We first established a preliminary predictive model that accounted for nonlinear soil response but our observations indicated insignificant improvements in inelastic spectral displacement estimations for constant strength or ductility. Hence, we decided to drop the soil nonlinearity in our GMPMs. Equation (1) shows the functional form used in our GMPMs.

$$\ln(Y) = a_1 + a_2[\min(M_w - 6.75, 0)] + a_3[\max(M_w - 6.75, 0)] + a_4(M_w - 8.5)^2 + a_5 F_N + a_6 F_R + [a_7 + a_8(M_w - 6.75)]\ln\left(\sqrt{{R_{JB}}^2 + {a_9}^2}\right) + a_{10}\ln\left(\frac{\min(V_{S30}, 1000)}{750}\right) + \varepsilon\sigma \quad (1)$$

The dependent parameter Y on the right hand side stands for the predicted inelastic spectral displacement, $S_{d,ie}$, ($S_{d,ie}^{Ry}$ for constant strength and $S_{d,ie}^{\mu}$ for constant ductility; unit is in meter) or inelastic-to-elastic spectral displacement ratio, C_{Ry} (for constant strength) and C_{μ} (for constant ductility). The natural logarithm of Y is estimated by a functional form consisting of event terms (quadratic bilinear magnitude scaling and style-of-faulting, SoF, scaling), distance term (magnitude dependent geometrical spreading) and linear site response term (from Sandikkaya et al., 2013). We assume linear site response as a function of V_{S30} with a constant site amplification for rock sites (V_{S30} = 1000 m/s) that is inherited from Sandikkaya et al. (2013). Considering the database in hand as well as the Sandikkaya et al. (2013) site model, the developed GMPMs have a magnitude coverage of 4.0 ≤ M_w ≤ 7.6, R_{JB} ≤ 200 and 150 m/s ≤ V_{S30} ≤ 1200 m/s.

The dependent (predictor) variables are moment magnitude (M_w), Joyner-Boore distance (R_{JB}), V_{S30} and the dummy variables for normal (F_N) and reverse (F_R) fault mechanisms. F_N and F_R are unity for normal and reverse faults, respectively, and zero otherwise. ε is the number of standard deviations and σ is the total standard deviation. We use random-effects algorithm (Abrahamson and Youngs, 1992) in regression analysis and the residuals (the difference between the natural logarithms of observed data and the median estimate) are decomposed into within-event and between-event residuals. The residuals are assumed to be normally distributed with zero mean and within-event (ϕ) and between-event (τ) standard deviations, respectively. The total standard deviation (sigma) is $\sigma = \sqrt{\phi^2 + \tau^2}$.

For inelastic spectral displacement predictive models, the SoF scaling and fictitious depth coefficients are adopted from ASB14. We did not observe any significant effect of SoF scaling and magnitude-dependent geometrical spreading scaling in inelastic-to-elastic spectral displacement ratio predictive models. Hence, regression coefficients a_5, a_6 and a_8 are set to zero for these GMPMs. We also observed that bilinear magnitude and magnitude-dependent geometric spreading coefficients are sensitive to the variations in R_y or μ values. We computed these coefficients from a single period and kept them the same for the rest of the spectral period range to obtain a smooth spectrum shape. For small R_y and μ values (≤ 3), these coefficients were computed from T = 0.15s – T = 0.2s band whereas for the rest of R_y and μ values the period band shifts to T = 0.4s.

The regression coefficients and corresponding standard deviations for each model are given in Appendix 1 for a limited set of period, R_y and μ. Appendix 2 lists the period-dependent correlation coefficients between inelastic-to-elastic spectral displacement ratio predictive models and the elastic spectral displacements. (We present the correlation coefficients only at the selected periods that are presented in Table A1). We compute the correlation coefficients by using the residuals of ASB14 (for elastic spectral response) and the proposed C_R and C_{μ} predictive models. They can be used to estimate more realistic inelastic displacements from C_R and C_{μ} predictive models. The full list of model regression coefficients as well as the correlation coefficients can be downloaded from the link:

https://drive.google.com/open?id=1B3qzbNaJi4IIDsTEQqMgSqhvvuyuMDKf.

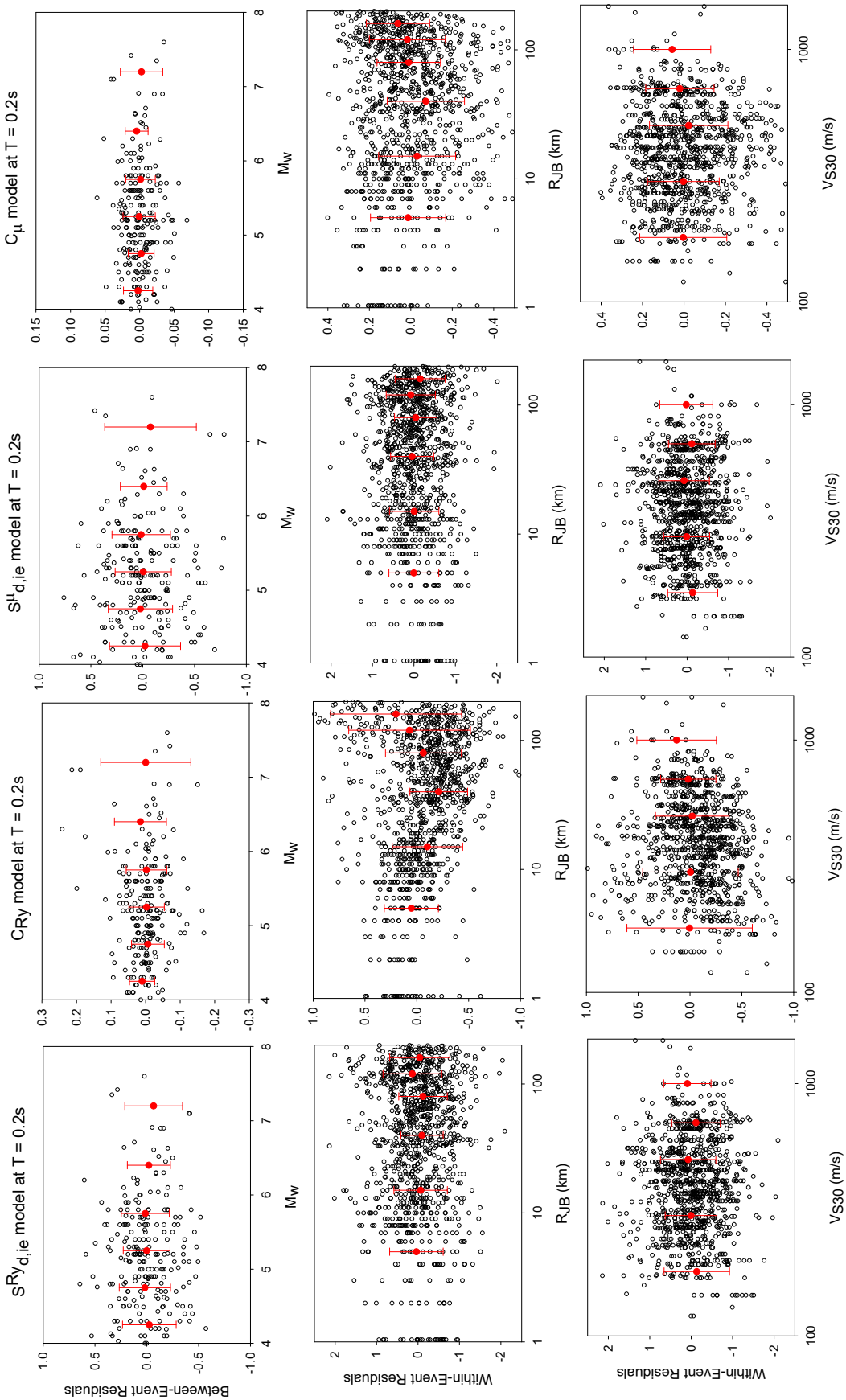

Figure 2. Residual distribution of the proposed models.

Figure 2 shows a sample set of residual scatters of the proposed GMPMs at T = 0.2s for R_y = 2 (panels in the first two columns) and μ = 2 (panels in the last two columns). The reason behind the choice of this period is that it shows the most biased residual trends within the entire period range of interest in this study. We plot the between-event residuals against M_w. These plots also show the variation of mean between-event residuals and ±1 standard deviations for between-event residual bins computed at different M_w intervals (0.5 units for $M_w \leq 6$ and 0.75 units for $M_w > 6$). The between-event residual plots for R_y and μ do not display significant trends in magnitude scaling. Therefore, the inelastic predictive models can properly account for the magnitude scaling. Similar plots of R_y and μ within-event residual scatters show unbiased trends in terms of V_{S30} suggesting the properness of linear site response assumption in the predictive models. The within-event residuals for source-to-site distance, R_{JB}, advocate an underestimation for C_R model for R_{JB} < 50 km whereas an overestimation for R_{JB} > 75 km.

Figure 3 presents the period dependent variation of total, between- and within-event standard deviations of all inelastic GMPMs. The standard deviation plots indicate $S_{d,ie}^{R_y}$ and $S_{d,ie}^{\mu}$ predictive models result in larger standard deviations with respect to C_R and C_μ GMPMs but the former models are not as sensitive as the latter models to the variations in R_y and μ. Figure 4 shows the period-dependent variation of correlation coefficients for C_R and C_μ predictive models. The correlation coefficients for C_R and C_μ display very similar trends with each other and they closely follow each other except for R_y = μ = 1.5 that represents the lowest level of nonlinearity among the chosen discrete R_y and μ values.

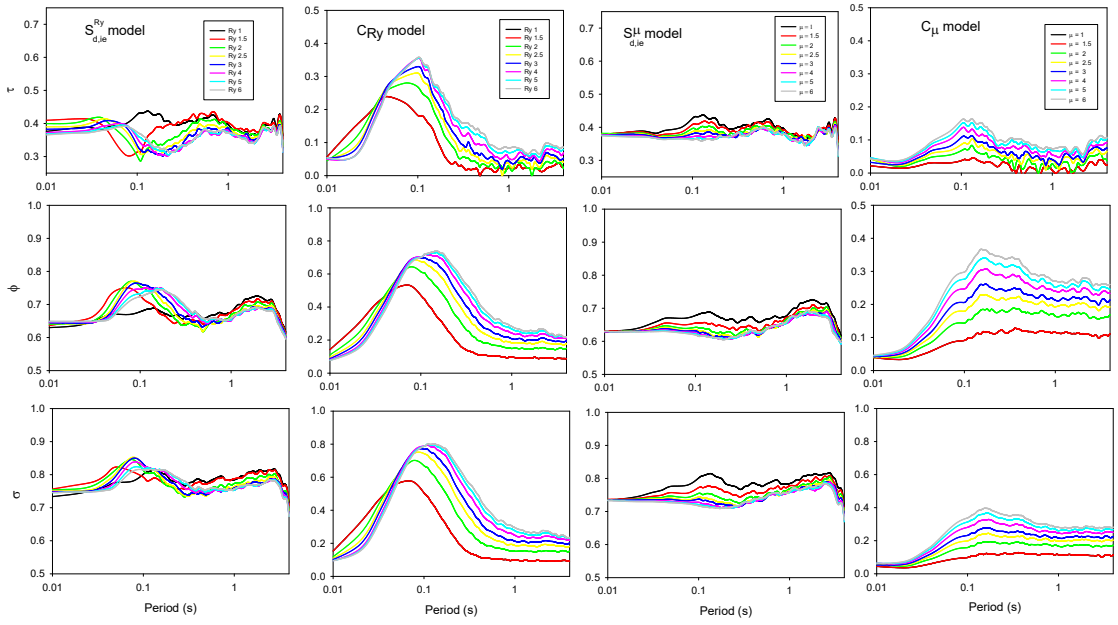

Figure 3. Period dependency of within-event, between-event and total standard deviations

Discussions on the Specific Features of the Proposed Models

We estimated the inelastic spectral displacements and inelastic-to-elastic spectral displacement ratios from the proposed predictive models by assuming a 90° dipping strike-slip fault rupturing at the surface. Figure 5 shows the magnitude effects (leftmost column panels), source-to-site distance effects (middle column panels) and site effects (rightmost column panels) on the inelastic GMPMs. There are four rows in Figure 5: the first and second rows display the median inelastic spectral displacement estimations for constant strength (R_y) and for constant ductility (μ), respectively whereas the third and fourth rows display the median inelastic-to-elastic spectral displacement ratio estimations for constant strength (R_y) and for constant ductility (μ),respectively.

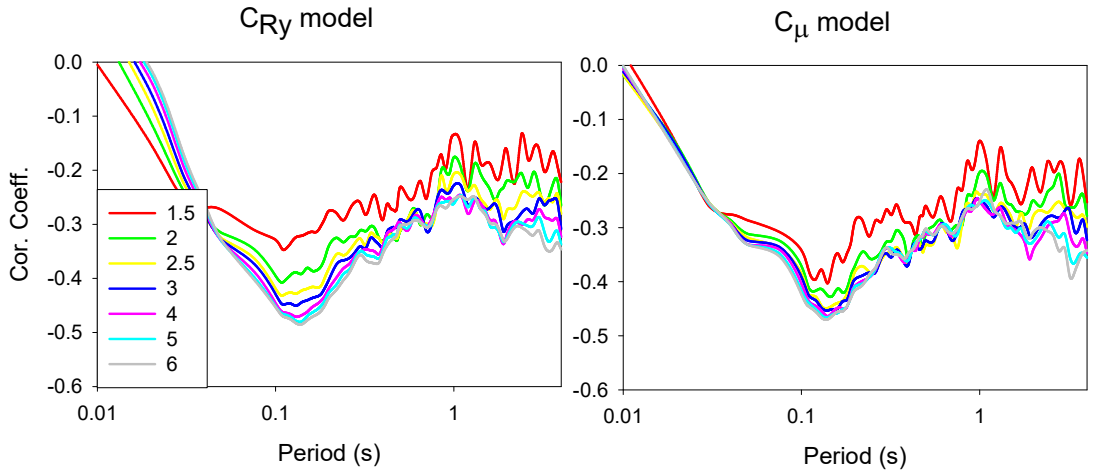

Figure 4. Period dependency of the correlation coefficients.

The plots display the variation of subject predictive models for T = 0.5 s. The earthquake scenarios in the leftmost column panels consider R_{JB} = 30 km whereas we assumed an earthquake of M_w 7.5 in the scenarios of the middle column panels. Both first and second column scenarios assumed a soft soil site characterized by V_{S30} = 200 m/s. The rightmost column panels display V_{S30} dependent site amplifications for an earthquake of M_w 7.5 and R_{JB} = 30 km to discuss the site effects on the inelastic GMPMs. We made the following observations from the inelastic GMPM estimations at different R_y and μ levels.

Magnitude effects:

- The increase in magnitude increases the inelastic deformation demands that are more prominent for larger R_y and μ,
- However, for magnitudes less than ~ M_w 4.7 inelastic spectral displacements are smaller than the elastic spectral displacement regardless of the R_y or μ value.

Distance effects:

- Since the selected magnitude scenario is large (M_w 7.5), increase in R_y or μ leads to larger inelastic spectral displacements with respect to their elastic counterpart.
- Larger inelastic spectral displacements with respect to their elastic counterparts for R_y or μ are more significant at large source-to site distances. This observation implies lower geometrical spreading with increasing R_y or μ and it is clearer in the median C_R and C_μ estimations. Note that although nonlinear deformation demands decrease gradually towards large distances, large C_R and C_μ values at such distances advocate the importance of accurate nonlinear deformation demand estimations with respect to their elastic counterparts. This way, the engineer would be able to make an optimum design to achieve the performance objectives dictated by the seismic design codes.
- The above comment is valid for sites dominated by large magnitude (M_w > 6) events that are more critical in seismic design.

Site effects:

- Site effect is reflected on to inelastic deformation measures (i.e., inelastic spectral displacement predictive models; $S_{d,ie}^{R_y}$ and $S_{d,ie}^{\mu}$ or inelastic-to-elastic displacement ratio predictive models; C_R and C_μ) in different modes. This observation is important because the current design code approach modifies site class corrected elastic spectral displacements by a C_R or C_μ type relationship. If such relationship fails to account for site effects properly, the resulting nonlinear deformation demands may not fully capture the soil behavior under earthquake excitation.
- Site amplification of nonlinear deformation demands increases with increasing R_y and μ for sites having $V_{S30} \leq 750$ m/s. However, for rock and very hard rock site conditions site effects reverse the trend and deamplification of inelastic deformation demands are observed for increasing R_y and μ.

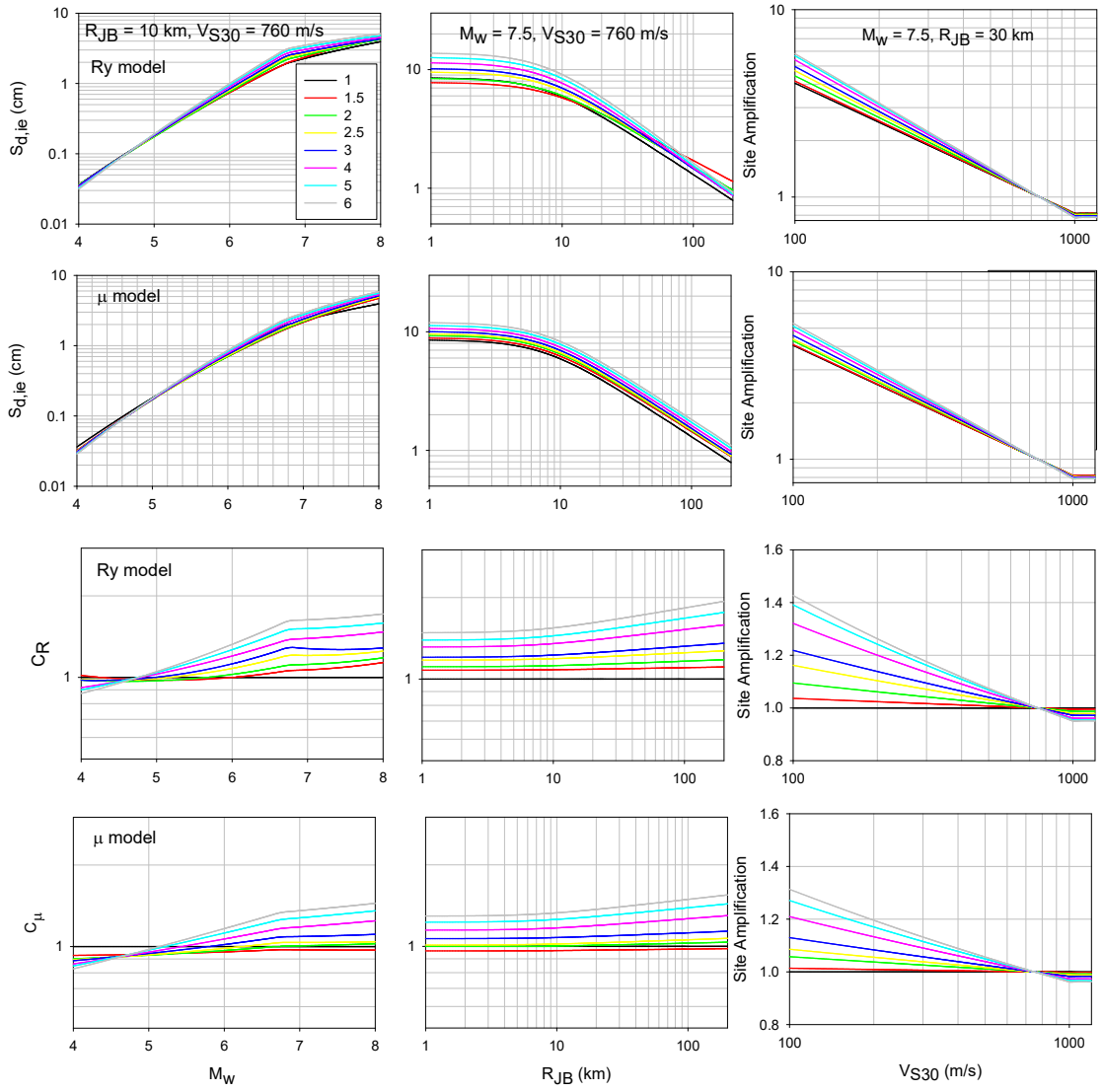

Figure 5. Magnitude, source-to-site distance and site effects on the proposed inelastic GMPMs.

Figure 6 presents the constant strength and constant ductility median inelastic displacement spectra (upper and lower panels, respectively in the left column) as well as period-dependent variation of median C_R and C_μ for a rock site (V_{S30} = 760 m/s) subjected to a M_w 7.5 strike-slip ground motion. The site is assumed to be located 10 km away from the horizontal projection of the ruptured fault plane (R_{JB} = 10 km). The inelastic displacement spectra suggest that spectral ordinates are rather more sensitive to the strength capacity (represented by R_y) than the ductility capacity (represented by μ) at very short and short periods ($T \leq 0.3$s). The difference between constant strength and constant ductility spectral displacements diminish after T = 0.3 s. One can make similar observations about the sensitivity to strength capacity from the comparisons of median C_R and C_μ curves. The sensitivity of strength capacity at short and very short periods leads to a more dispersive inelastic spectral displacement behavior in $S_{d,ie}^{R_y}$ spectra. This is expected since $S_{d,ie}^{R_y}$ spectral ordinates are directly computed for a given strength capacity (i.e., R_y) without any constraint. Note that both C_R and C_μ curves attain values less or equal to unity after T = 3 s, which means lower inelastic deformation demands with respect to their elastic counterparts for regardless of R_y or μ value. The engineering community generally refers to this phenomenon as equal displacement rule. As we have already discussed it in Figure 5, equal displacement rule (EDR) is mainly controlled by magnitude and level of inelasticity (i.e., up and down scaling of R_y and μ) that is further evaluated in Figure 7.

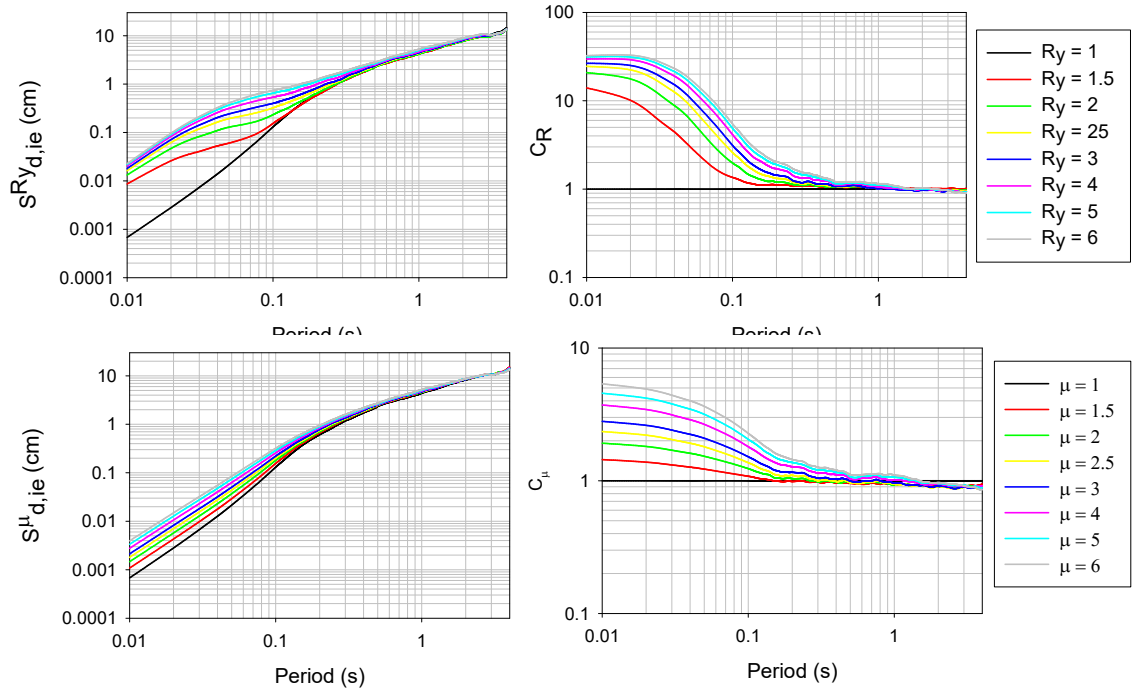

Figure 6. Median inelastic spectral displacement estimations for constant strength and for constant ductility in the upper and lower left panels, respectively for a M_w 7.5 strike-slip ground motion (R_{JB} = 10 km). Corresponding median CR and Cμ estimations in the upper right and lower right panels, respectively.

The left panel in Figure 7 presents median C_R estimations of R_y = 1.5 and R_y = 4 for M_w 6 and M_w 7.5 strike-slip ground motions at a soft site (V_{S30} = 300 m/s) located R_{JB} = 20 km from the ruptured fault surface. The median C_R trends indicate that EDR is primarily controlled by magnitude (large M_w shifts the commencement of EDR to longer periods) that is followed by the level of inelasticity (EDR becomes applicable at longer periods when R_y attains larger values). The right panel in Figure 7 shows the median C_R estimations of R_y = 1.5 and R_y = 4 for two site conditions (V_{S30} = 200 m/s vs. V_{S30} = 760 m/s) for a strike-slip earthquake of M_w 7 and R_{JB} = 10 km. The median C_R trends indicate that site effect is also as prominent as magnitude and the level of inelasticity in EDR such that softer sites shifts the spectral periods for the commencement of EDR. We note that in many modern seismic design codes the provided C_R (or C_{μ}) formulations disregard the magnitude effect for the implementation of EDR, which seems to be an important deficiency for accurate estimation of the inelastic spectral displacements.

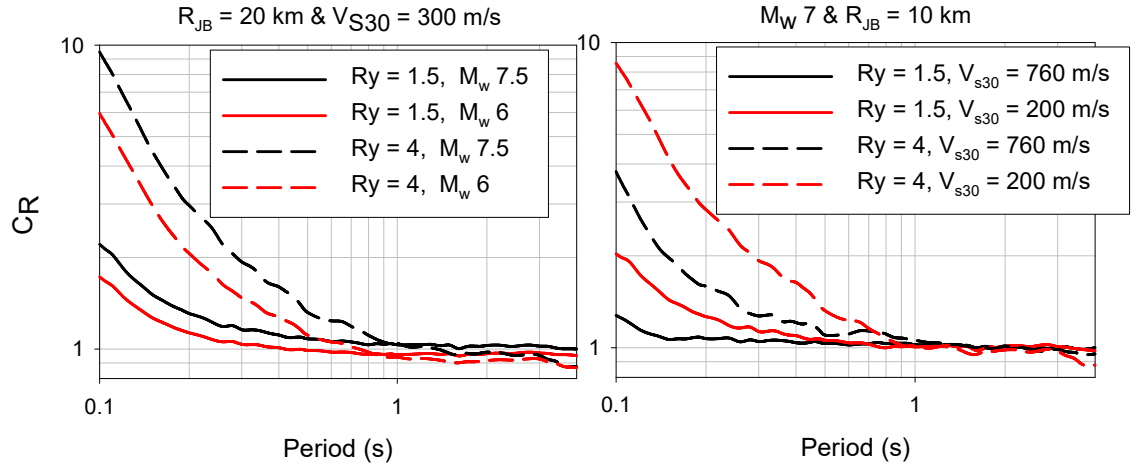

Figure 7. Magnitude, inelastic level and site condition dependency of equal displacement rule

The C_R estimates of FEMA 440 (FEMA, 2005), Ruiz-Garcia and Miranda (RM2003; 2003), Tothong and Cornell (TC06; 2006) and Stafford et al. (S2016; 2016) are compared with our proposed model to convey a preliminary information about the model uncertainty in inelastic-to-elastic spectral displacement ratio predictions. Note that FEMA 440 and RM2003 models are independent of magnitude whereas the rest of the C_R predictive models use magnitude as an estimator parameter. We compare the models for strike-slip earthquakes of M_w 7.5 and M_w 5.5. The source-to site distance value and site condition are chosen as R_{JB} = 20 km and V_{S30} = 270 m/s, respectively. The left panel in Figure 7 shows the comparative plots for M_w 7.5 and the right panel shows the same comparisons for M_w 5.5. Among the magnitude independent C_R predictive models, FEMA 440 has an increasing trend between $1 \leq R_y \leq 3$ that is followed by a constant value whereas the other magnitude independent predictive model RM2003 estimates increasing C_R as R_y increases. The median C_R predictions of the proposed model are higher than those of TC06 and S2016 models for M_w 5.5. The proposed model predicts similar median C_R values with S2016 at M_w 7.5 whereas our median C_R estimations for the same magnitude are higher with respect to the ones in TC06. The limited discussions about Figure 7 emphasize the modelling differences in inelastic GMPMs that may result in significant discrepancies in structural deformation demands. Besides, the comparative plots once again advocate the importance of magnitude scaling in the development of inelastic GMPMs whose absence would result in very conservative or unsafe deformation demands depending on the most contributing earthquake to the seismic hazard.

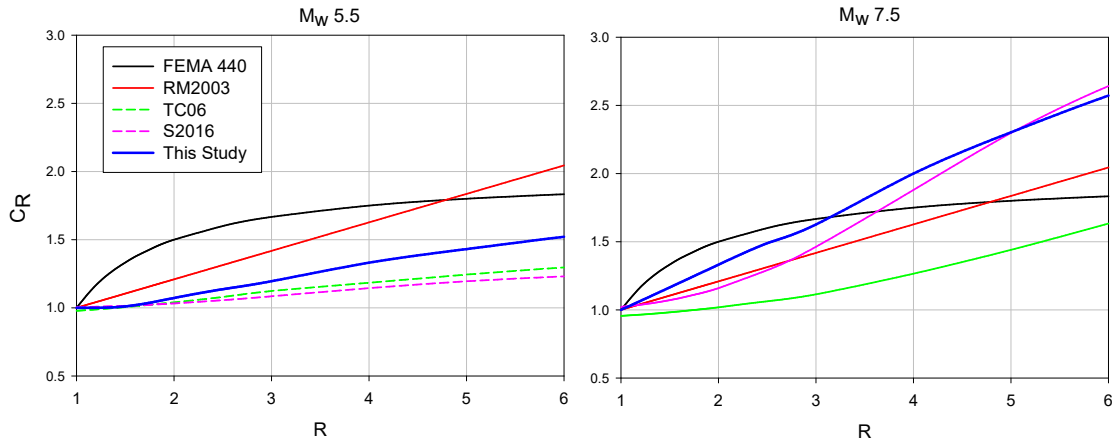

Figure 8. Comparisons of C_R predictive models.

Implementation of Proposed GMPMs to PSHA

The current code-based approach modifies elastic spectral displacement demands at a specific return period (e.g., 475-year or 2475-year return period) for inelastic displacements via deterministic expressions. The engineer uses the computed inelastic spectral displacement to estimate the structural deformation(s) for that return period, which corresponds to a specific performance level dictated in the code. The elastic spectral displacement demands are determined from the code design spectrum that is generally the representative of the uniform hazard spectrum (product of the PSHA process). The deterministic expressions for modifying these probabilistic elastic spectral displacements are similar to those presented in the previous section (e.g., FEMA 440 equations or simplified versions of RM2003).

We implemented the proposed predictive models to estimate inelastic spectral displacements at different return periods for a fictitious case. Our objective is to make some limited observations on how different approaches would affect the computation of $S_{d,ie}$ and how they compare with the conventional code approach as described briefly in the above paragraph. We considered the constant strength GMPMs that estimate $S_{d,ie}^{R_y}$ and C_R. The later model requires the convolution with another predictive model that estimates elastic displacement spectrum. We describe the theoretical background of the PSHA computations in the following.

The use of direct $S_{d,ie}^{R_y}$ predictive model in PSHA is the application of conventional Cornell (1968) approach (Equation 2). The annual exceedance rate of $S_{d,ie}$ exceeding a threshold level (MRE_Z)

is the integral of the product of exceedance probability of $S_{d,ie}$ conditioned on a given magnitude-distance pair ($Pr[Z > z|m,r]$) and their occurrence probabilities ($f_M(m)$ and $f_R(r)$) over a predetermined magnitude and distance range. In Equation 2, $S_{d,ie}$ is represented by Z and λ_0 is minimum activity rate.

$$MRE_Z = \lambda_0 \int_m \int_r Pr[Z > z|m,r] f_M(m) f_R(r) dm\, dr \quad (2)$$

In Equation (2), $Pr[Z > z|m,r]$ is obtained from the proposed $S_{d,ie}^{R_y}$ GMPM. Equation (2) can also be used to compute the annual exceedance rate of elastic spectral displacement X as given in Equation (3)

$$MRE_X = \lambda_0 \int_m \int_r Pr[X > x|m,r] f_M(m) f_R(r) dm\, dr \quad (3)$$

$Pr[X > x|m,r]$ is determined from a GMPM that estimates the elastic spectral displacement (e.g., Akkar et al., 2014a). The derivative of MRE_X is annual exceedance rate density, MRD_X and its convolution with the exceedance probability of C_R conditioned on a magnitude and distance pair would once again give annual exceedance rate of inelastic spectral displacement, MRE_Z. This approach is called as convolution approach (Bazzuro and Cornell, 2004) and it is given in Equation (4).

$$MRE_Z = \int Pr[Y > y|x] MRD_x\, dx \quad (4)$$

In Equation (4), $Pr[Y > y|x]$ is the exceedance probability of C_R (denoted by Y) conditioned on the occurrence of a specific elastic spectral displacement vale (denoted by x). The conventional PSHA (direct implementation of $S_{d,ie}^{R_y}$ GMPM) and the convolution approach (implementation of C_R GMPM together with Akkar et al., 2014a) are used for a fictitious site located 20 km away from the center of a 90° dipping strike-slip fault. The fault is assumed to have a length of 150 km and its down dip width is 10 km. The characteristic earthquake magnitude of this fault segment is determined as M_w 7.35 from Wells and Coppersmith (1994) and we used characteristic recurrence model by Youngs and Coppersmith (1985) for stochastic earthquake modeling. In all calculations the site class is taken as V_{S30} = 760 m/s.

Figure 9 shows the inelastic spectral displacement hazard curves computed from conventional PSHA and convolution approach for two spectral ordinates (T = 0.2s and T = 1.0s) and R_y = 4. For completeness the elastic displacement spectrum hazard curve is also given that is computed from Akkar et al. (2014a). The comparisons suggest that conventional and convolution PSHA approaches would show some discrepancies in estimating inelastic spectral displacements. In the most general sense, the conventional PSHA would draw the upper bound at lower return periods and the lower bound for larger return periods.

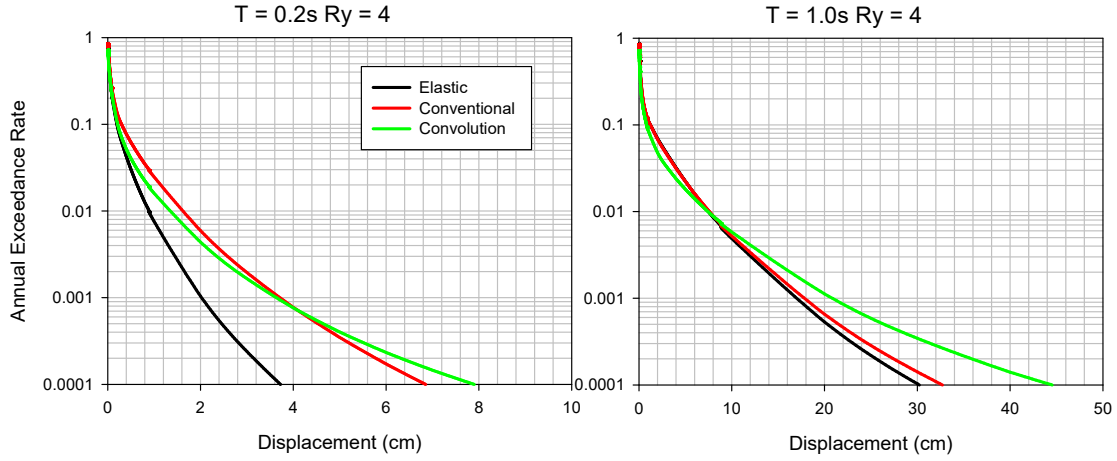

Figure 9. Comparison of inelastic displacement demands from different hazard approaches.

Comparisons in Figure 10 show the entire inelastic displacement spectra computed from conventional and convolution PSHA for R_y = 4. The same fictitious case was used in the calculations and the spectral plots are given for 475-year and 2475-year return periods (left and

right panels in Figure 10, respectively). The panels in Figure 10 also show the representative inelastic displacement spectra that are computed by modifying the uniform hazard elastic displacement spectra with the deterministic inelastic-to-elastic spectral displacement ratio expression in FEMA 440. The comparisons suggest that the discrepancy between conventional and convolution approaches are more prominent for 2475-year return period. The convolution PSHA results would constitute the upper bound towards longer periods that are significantly large for 2475-year return period. The deterministic FEMA 440 expressions follow closely the conventional PSHA results for this case study however further studies should be executed to cast a reliable conclusion about the consistency and sufficiency of code-based deterministic formulations in the estimation of inelastic deformation demands.

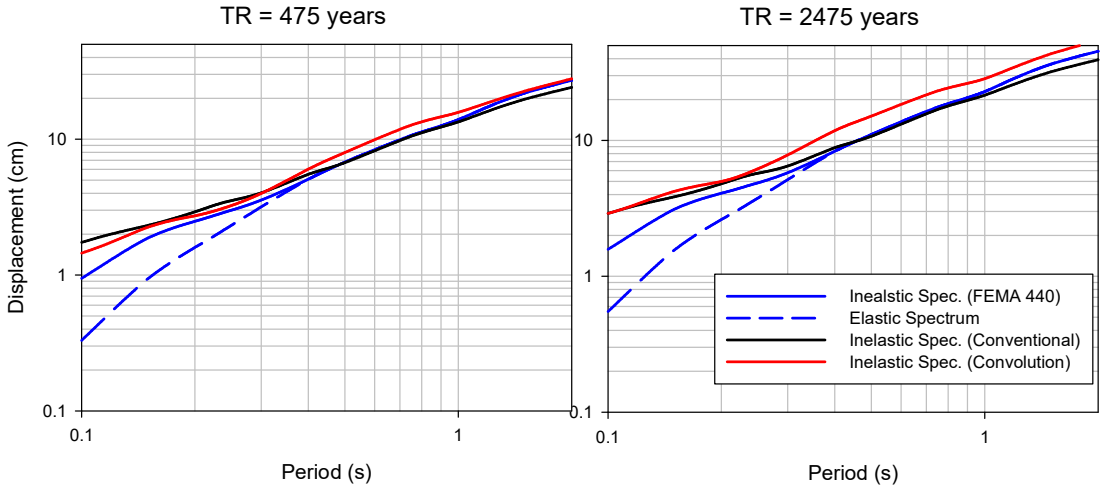

Figure 10. Comparison of estimated spectral displacements from the proposed predictive models and a typical seismic code approach

Conclusions

We present two sets of inelastic GMPMs for strength reduction factor (R_y) and ductility (μ) to estimate 5%-damped inelastic spectral displacements. The first set of predictive models directly estimate inelastic spectral displacement for a given earthquake scenario ($S_{d,ie}^{R_y}$ model for constant strength and $S_{d,ie}^{\mu}$ model for constant ductility). The second suit of GMPMs estimate inelastic-to-elastic spectral displacement ratios (C_R model for constant strength and C_μ model for constant ductility) and require elastic spectral displacement that is representative of the same earthquake scenario to predict $S_{d,ie}$. The models are developed for a bilinear hysteretic model with a post yield stiffness ratio of 3%. The database we used to develop the GMPMs is a version of pan-European ground-motion database. The models are valid for magnitudes between $4 \leq M_w \leq 8$ and for distances $R_{JB} \leq 200$ km. They assume linear site amplification as a function of V_{S30} and can account for $S_{d,ie}$ amplitude differences due to style of faulting (valid property only for $S_{d,ie}^{R_y}$ and $S_{d,ie}^{\mu}$ models).

The developed GMPMs advocate the importance of magnitude, source-to-site distance and site conditions in inelastic spectral displacements. Large magnitude events and soft sites increase the inelastic spectral displacement demands. Larger source-to-site distances would yield higher inelastic-to-elastic spectral displacements. The inelastic spectral displacements are very sensitive to the variations in R_y at short and very short periods when compared to their sensitivity to the changes in displacement ductility in the same period range. As spectral periods shifts towards longer periods both constant strength and constant ductility displacement spectra start converging each other.

The comparisons of inelastic spectral displacements computed after the implementation of proposed GMPMs in PSHA suggest larger spectral demands by C_R and C_μ models than those determined from $S_{d,ie}^{R_y}$ and $S_{d,ie}^{\mu}$ GMPMs. This observation is rather valid towards longer spectral periods and discrepancies become prominent at larger return periods (i.e., 2475-year in our case study). The code-based approach that modifies elastic displacement spectrum by deterministic

C_R or C_μ relationships may result in different inelastic spectral estimates with respect to the GMPMs proposed in this paper. Our current case studies show that code-based inelastic spectral displacement estimations may be lower than those computed from the proposed inelastic models.

References

Abrahamson NA and Youngs RR (1992), A stable algorithm for regression analyses using the random effects model, Bull Seismol Soc Am, 82:505–510

Akkar S, Sandıkkaya MA, Senyurt M, Azari Sisi A, Ay BO, Treversa P, Douglas J, Cotton F, Luzi L, Hernandez B and Godey S (2014a), Reference database for seismic ground-motion in Europe (RESORCE), Bull Earthq Eng, 12:311–339

Akkar S, Sandıkkaya MA and Bommer JJ (2014b), Empirical ground-motion models for point- and extended source crustal earthquake scenarios in Europe and the Middle East, Bull Earthq Eng, 12:359–387

Akkar S, Sandıkkaya MA and Ay MO (2014c), Compatible ground-motion prediction equations for damping scaling factors and vertical-to-horizontal spectral amplitude ratios for the broader Europe region, Bull Earthq Eng, 12:517–547

Applied Technology Council (ATC). Evaluation and improvement of inelastic seismic analysis procedures. Report FEMA-440, Federal Emergency Management Agency, Washington, DC, 2005

ASCE. American Society of Civil Engineers (2016), Minimum design loads for buildings and other structures. Reston, Virginia: ASCE/SEI.

Aslani H and Miranda E (2005), Probabilistic earthquake loss estimation and loss disaggregation in buildings, John A. Blume Earthquake Engineering Center Technical Report No. 157. Stanford University, Stanford, CA.

Bazzurro P and Cornell CA)2004), Nonlinear soil-site effects in probabilistic seismic hazard analysis, Bull Seismol Soc Am, 94.6:2110–23.

Bozorgnia Y, Hachem MM and Campbell KW (2010), Ground motion prediction equation (“attenuation relationship”) for inelastic response spectra, Earthquake Spectra, 26(1):1–23.

Cornell CA (1968), Engineering seismic risk analysis, Bull Seismol Soc Am, 58 (5): 1583-1606.

Çağnan Z, Akkar S, Kale Ö and Sandıkkaya A (2017), A model for predicting vertical component peak ground acceleration (PGA), peak ground velocity (PGV), and 5% damped pseudo-spectral acceleration (PSA) for Europe and the Middle East, Bulletin of Earthquake Engineering, 15(7):2617-2643.

Chopra AK and Chintanapakdee C (2004), Inelastic deformation ratios for design and evaluation of structures: Single-degree-of-freedom bilinear systems, Journal of Structural Engineering, 130(9):1309–1319.

Heresi P, Davalos H and Miranda E (2018), Ground Motion Prediction Model for the Peak Inelastic Displacement of Single-Degree-of-Freedom Bilinear Systems, Earthquake Spectra, 34(3):1177–1199.

Iwan WD (1980), Estimating inelastic response spectra from elastic spectra, Earthquake Engineering & Structural Dynamics, 8(4): 375–388.

Iwan WD and Guyader AC (2002). A study of the accuracy of the capacity spectrum method in engineering analysis, in Proceedings, 3rd US-Japan Workshop on Performace-Based Earthquake Engineering Methodology for Reinforced Concrete Building Structures, Pacific Earthquake Eng. Research Center, 16-18 August 2001, Seattle, Washington, 86–102.

Luco N and Cornell CA (2007), Structure-specific scalar intensity measures for near-source and ordinary earthquake ground motions, Earthquake Spectra, 23(2): 357–392.

Luco N, Mori Y, Funahashi Y, Cornell CA and Nakashima M (2003), Evaluation of predictors of non-linear seismic demands using “fishbone” models of SMRF buildings, Earthquake Engineering & Structural Dynamics, 32(14): 2267–2288.

Miranda E, Aslani H and Taghavi S (2004), Assessment of seismic performance in terms of economic losses, in Proceedings, International Workshop on Performance-Based Seismic Design: Concepts and Implementation, 28 June - 1 July 2004, Bled, Slovenia, 149–160.

Newmark NM, Hall WJ.(1982), Earthquake Spectra and Design. Earthquake Engineering Research Institute, Berkeley, CA.

Ruiz-Garcia and Miranda E (2003), Inelastic displacement ratios for evaluation of existing structures, Earthquake Engineering and Structural Dynamics, 32(9): 1237-1258.

Sandıkkaya MA and Akkar S (2017), Cumulative Absolute Velocity, Arias Intensity and Significant Duration Predictive Models from a Global Pan-European Strong-Motion Dataset, Bulletin of Earthquake Engineering, 15: 1881-1898

Sandıkkaya MA, Akkar S and Bard P-Y (2013) A nonlinear site amplification model for the new pan-European ground-motion prediction equations, Bull Seismol Soc Am, 103:19–32

Stafford PJ, Sullivan TJ, and Pennucci D (2016), Empirical correlation between inelastic and elastic spectral displacement demands, Earthquake Spectra 32(3):1419–1448.

Turkish Earthquake Code, TEC (2019).

Tothong P and Cornell CA (2006), An Empirical Ground-Motion Attenuation Relation for Inelastic Spectral Displacement, Bull Seismol Soc Am, 96(6): 2146-2164.

Wells DL and Coppersmith KJ (1994), New empirical relationships among magnitude, rupture length, rupture width, rupture area, and surface displacement, Bull Seismol Soc Am, 84:974–1002

Youngs RR and Coppersmith KJ (1985) Implications of fault slip rates and earthquake recurrence models to probabilistic seismic hazard estimates, Bull Seismol Soc Am, 75(4):939–64.

Appendix 1: Regression coefficients and standard deviations of the inelastic GMPMs

$S_{d,ie}^{Ry}$ $model\ for\ Ry = 2$

Periods (s)	a_1	a_2	a_3	a_4	a_5	a_6	a_7	a_8	a_9	a_{10}	τ	φ
0.1	-4.0438	0.2936	-0.5029	-0.0056	-0.0749	0.0761	-0.8491	0.2731	7.5	-0.6585	0.302	0.754
0.15	-3.2865	0.2936	-0.5029	0.002	-0.0265	0.0545	-0.9194	0.2731	7.5	-0.533	0.348	0.713
0.2	-2.787	0.2936	-0.5029	0.0003	0	0.0493	-0.9469	0.2731	7.5	-0.5216	0.34	0.684
0.3	-2.2443	0.2936	-0.5029	-0.0113	0	0.0469	-0.9235	0.2731	7.5	-0.5561	0.369	0.637
0.5	-1.6955	0.2936	-0.5029	-0.0418	0	0.0271	-0.8662	0.2731	7.5	-0.7389	0.414	0.619
0.75	-1.4837	0.2936	-0.5029	-0.0693	0	0.0141	-0.778	0.2731	7.5	-0.8678	0.408	0.648
1	-1.3778	0.2936	-0.5029	-0.0861	0	0	-0.727	0.2731	7.5	-0.9532	0.388	0.669
1.5	-1.1034	0.2936	-0.5029	-0.1123	0	0	-0.6777	0.2731	7.5	-0.9764	0.37	0.697
2	-0.863	0.2936	-0.5029	-0.1301	0	-0.009	-0.6712	0.2731	7.5	-0.9741	0.365	0.707
3	-0.7185	0.2936	-0.5029	-0.148	0	-0.0683	-0.6434	0.2731	7.5	-0.955	0.375	0.69
4	-0.3654	0.2936	-0.5029	-0.1737	0	-0.2231	-0.6384	0.2731	7.5	-0.8412	0.329	0.604

$S_{d,ie}^{Ry}$ $model\ for\ Ry = 4$

Periods (s)	a_1	a_2	a_3	a_4	a_5	a_6	a_7	a_8	a_9	a_{10}	τ	φ
0.1	-2.9823	0.5408	-0.37	-0.0428	-0.0749	0.0761	-0.8959	0.184	7.5	-0.7609	0.355	0.746
0.15	-2.6073	0.5408	-0.37	-0.042	-0.0265	0.0545	-0.9159	0.184	7.5	-0.7421	0.316	0.75
0.2	-2.2361	0.5408	-0.37	-0.0433	0	0.0493	-0.9465	0.184	7.5	-0.7141	0.304	0.732
0.3	-1.8393	0.5408	-0.37	-0.0473	0	0.0469	-0.9447	0.184	7.5	-0.7354	0.321	0.684
0.5	-1.341	0.5408	-0.37	-0.0677	0	0.0271	-0.9244	0.184	7.5	-0.8367	0.366	0.648
0.75	-1.0692	0.5408	-0.37	-0.0925	0	0.0141	-0.861	0.184	7.5	-0.896	0.366	0.657
1	-0.9324	0.5408	-0.37	-0.1067	0	0	-0.822	0.184	7.5	-0.9377	0.379	0.651
1.5	-0.6388	0.5408	-0.37	-0.1299	0	0	-0.793	0.184	7.5	-0.9474	0.361	0.68
2	-0.3989	0.5408	-0.37	-0.1479	0	-0.009	-0.7853	0.184	7.5	-0.9431	0.345	0.69
3	-0.205	0.5408	-0.37	-0.164	0	-0.0683	-0.7756	0.184	7.5	-0.9307	0.375	0.68
4	0.0498	0.5408	-0.37	-0.1847	0	-0.2231	-0.7601	0.184	7.5	-0.8016	0.312	0.599

$S_{d,ie}^{\mu}$ $model\ for\ \mu = 2$

Periods (s)	a_1	a_2	a_3	a_4	a_5	a_6	a_7	a_8	a_9	a_{10}	τ	φ
0.1	-3.4448	-0.2139	-0.3184	-0.0548	-0.0749	0.0761	-1.209	0.2509	7.5	-0.2355	0.396	0.642
0.15	-2.7097	-0.2139	-0.3184	-0.0651	-0.0265	0.0545	-1.1579	0.2509	7.5	-0.2771	0.403	0.63
0.2	-2.3274	-0.2139	-0.3184	-0.0763	0	0.0493	-1.1008	0.2509	7.5	-0.345	0.386	0.624
0.3	-1.9638	-0.2139	-0.3184	-0.0962	0	0.0469	-0.9979	0.2509	7.5	-0.4867	0.376	0.624
0.5	-1.518	-0.2139	-0.3184	-0.1298	0	0.0271	-0.9011	0.2509	7.5	-0.7216	0.405	0.619
0.75	-1.3345	-0.2139	-0.3184	-0.1572	0	0.0141	-0.8088	0.2509	7.5	-0.8696	0.399	0.647
1	-1.2316	-0.2139	-0.3184	-0.1741	0	0	-0.7521	0.2509	7.5	-0.9382	0.385	0.666
1.5	-0.9332	-0.2139	-0.3184	-0.2021	0	0	-0.7098	0.2509	7.5	-0.9773	0.369	0.689
2	-0.6958	-0.2139	-0.3184	-0.2192	0	-0.009	-0.7033	0.2509	7.5	-0.9677	0.366	0.701
3	-0.5097	-0.2139	-0.3184	-0.239	0	-0.0683	-0.6801	0.2509	7.5	-0.9377	0.38	0.684
4	-0.1597	-0.2139	-0.3184	-0.264	0	-0.2231	-0.6775	0.2509	7.5	-0.8308	0.334	0.601

$S_{d,ie}^{\mu}$ $model\ for\ \mu = 4$

Periods (s)	a_1	a_2	a_3	a_4	a_5	a_6	a_7	a_8	a_9	a_{10}	τ	φ
0.1	-3.1682	-0.0409	-0.3088	-0.0533	-0.0749	0.0761	-1.1643	0.2285	7.5	-0.326	0.372	0.626
0.15	-2.5281	-0.0409	-0.3088	-0.0649	-0.0265	0.0545	-1.1189	0.2285	7.5	-0.3827	0.373	0.613
0.2	-2.1866	-0.0409	-0.3088	-0.0776	0	0.0493	-1.0696	0.2285	7.5	-0.4602	0.372	0.608
0.3	-1.8436	-0.0409	-0.3088	-0.0963	0	0.0469	-0.9819	0.2285	7.5	-0.5756	0.377	0.614
0.5	-1.4498	-0.0409	-0.3088	-0.1272	0	0.0271	-0.899	0.2285	7.5	-0.7882	0.392	0.622
0.75	-1.2342	-0.0409	-0.3088	-0.1539	0	0.0141	-0.8114	0.2285	7.5	-0.8731	0.382	0.649
1	-1.0919	-0.0409	-0.3088	-0.1688	0	0	-0.772	0.2285	7.5	-0.9191	0.383	0.655
1.5	-0.8153	-0.0409	-0.3088	-0.192	0	0	-0.7407	0.2285	7.5	-0.9416	0.358	0.68
2	-0.5539	-0.0409	-0.3088	-0.2091	0	-0.009	-0.7402	0.2285	7.5	-0.94	0.357	0.679
3	-0.3707	-0.0409	-0.3088	-0.2251	0	-0.0683	-0.7311	0.2285	7.5	-0.9379	0.388	0.676
4	-0.0215	-0.0409	-0.3088	-0.2496	0	-0.2231	-0.7277	0.2285	7.5	-0.7977	0.319	0.59

C_{Ry} *model for* $Ry = 2$

Periods (s)	a_1	a_2	a_3	a_4	a_5	a_6	a_7	a_8	a_9	a_{10}	τ	φ
0.1	-0.4404	0.2351	0.1162	-0.0169	0	0	0.4189	0	7.5	-0.5049	0.268	0.614
0.15	-0.5482	0.2351	0.1162	0.0008	0	0	0.2919	0	7.5	-0.3632	0.195	0.522
0.2	-0.3393	0.2351	0.1162	0.0097	0	0	0.1689	0	7.5	-0.2476	0.118	0.429
0.3	-0.1878	0.2351	0.1162	0.0206	0	0	0.0721	0	7.5	-0.1421	0.053	0.279
0.5	-0.108	0.2351	0.1162	0.0301	0	0	0.0182	0	7.5	-0.0449	0.034	0.183
0.75	-0.0681	0.2351	0.1162	0.0335	0	0	0.0068	0	7.5	0.0357	0.024	0.164
1	-0.1221	0.2351	0.1162	0.0371	0	0	0.0041	0	7.5	0.0175	0.028	0.149
1.5	-0.1396	0.2351	0.1162	0.0396	0	0	0.0041	0	7.5	0.0109	0.032	0.148
2	-0.0967	0.2351	0.1162	0.0401	0	0	-0.013	0	7.5	-0.0122	0.023	0.15
3	-0.1717	0.2351	0.1162	0.0447	0	0	0.0005	0	7.5	-0.0125	0.039	0.142
4	-0.17	0.2351	0.1162	0.0456	0	0	0.0034	0	7.5	0.0377	0.021	0.151

C_{Ry} *model for* $Ry = 4$

Periods (s)	a_1	a_2	a_3	a_4	a_5	a_6	a_7	a_8	a_9	a_{10}	τ	φ
0.1	0.1727	0.2728	0.0948	-0.0362	0	0	0.484	0	7.5	-0.613	0.355	0.704
0.15	-0.3176	0.2728	0.0948	-0.0257	0	0	0.411	0	7.5	-0.5646	0.266	0.71
0.2	-0.2371	0.2728	0.0948	-0.0166	0	0	0.2852	0	7.5	-0.4327	0.205	0.64
0.3	-0.1753	0.2728	0.0948	0.0006	0	0	0.1561	0	7.5	-0.312	0.127	0.489
0.5	-0.1169	0.2728	0.0948	0.0198	0	0	0.0574	0	7.5	-0.1382	0.093	0.327
0.75	-0.0156	0.2728	0.0948	0.0255	0	0	0.0218	0	7.5	0.0091	0.056	0.271
1	-0.0713	0.2728	0.0948	0.0328	0	0	0.0119	0	7.5	0.0296	0.053	0.243
1.5	-0.081	0.2728	0.0948	0.0398	0	0	-0.0085	0	7.5	0.0403	0.06	0.227
2	-0.0501	0.2728	0.0948	0.0404	0	0	-0.0222	0	7.5	0.0191	0.053	0.233
3	-0.0749	0.2728	0.0948	0.0473	0	0	-0.0273	0	7.5	0.0093	0.08	0.21
4	-0.1283	0.2728	0.0948	0.0511	0	0	-0.0231	0	7.5	0.0625	0.069	0.209

$C_{R\mu}$ *model for* $\mu = 2$

Periods (s)	a_1	a_2	a_3	a_4	a_5	a_6	a_7	a_8	a_9	a_{10}	τ	φ
0.1	-0.0363	0.0701	0.0278	-0.0019	0	0	0.0905	0	7.5	-0.0995	0.068	0.143
0.15	-0.1949	0.0701	0.0278	-0.0018	0	0	0.0918	0	7.5	-0.1242	0.063	0.182
0.2	-0.1359	0.0701	0.0278	-0.0018	0	0	0.0613	0	7.5	-0.0851	0.047	0.186
0.3	-0.1328	0.0701	0.0278	0.0002	0	0	0.0383	0	7.5	-0.0789	0.045	0.178
0.5	-0.0876	0.0701	0.0278	0.005	0	0	0.0114	0	7.5	-0.0278	0.02	0.176
0.75	-0.0576	0.0701	0.0278	0.0079	0	0	0.0005	0	7.5	0.0329	0.024	0.177
1	-0.1142	0.0701	0.0278	0.0113	0	0	0.0039	0	7.5	0.0309	0.028	0.164
1.5	-0.12	0.0701	0.0278	0.013	0	0	-0.0011	0	7.5	0.0118	0.029	0.172
2	-0.0857	0.0701	0.0278	0.0143	0	0	-0.0182	0	7.5	-0.0063	0.025	0.173
3	-0.1194	0.0701	0.0278	0.0177	0	0	-0.0099	0	7.5	0.0039	0.053	0.155
4	-0.1143	0.0701	0.0278	0.0189	0	0	-0.0115	0	7.5	0.0429	0.037	0.169

$C_{R\mu}$ *model for* $\mu = 4$

Periods (s)	a_1	a_2	a_3	a_4	a_5	a_6	a_7	a_8	a_9	a_{10}	τ	φ
0.1	0.1384	0.1439	0.0635	-0.0027	0	0	0.1621	0	7.5	-0.1878	0.134	0.247
0.15	-0.1205	0.1439	0.0635	-0.0038	0	0	0.1599	0	7.5	-0.2231	0.114	0.303
0.2	-0.1007	0.1439	0.0635	-0.0053	0	0	0.1205	0	7.5	-0.1954	0.102	0.294
0.3	-0.1254	0.1439	0.0635	-0.0018	0	0	0.084	0	7.5	-0.1628	0.073	0.282
0.5	-0.1159	0.1439	0.0635	0.0054	0	0	0.0376	0	7.5	-0.0945	0.083	0.263
0.75	-0.0415	0.1439	0.0635	0.0082	0	0	0.0225	0	7.5	0.0318	0.05	0.254
1	-0.0769	0.1439	0.0635	0.0145	0	0	0.0101	0	7.5	0.0477	0.055	0.241
1.5	-0.0921	0.1439	0.0635	0.0205	0	0	-0.0084	0	7.5	0.0446	0.061	0.246
2	-0.0513	0.1439	0.0635	0.0229	0	0	-0.0287	0	7.5	0.0226	0.06	0.248
3	-0.0903	0.1439	0.0635	0.0297	0	0	-0.0328	0	7.5	0.0035	0.084	0.228
4	-0.0753	0.1439	0.0635	0.0309	0	0	-0.0365	0	7.5	0.07	0.091	0.234

Appendix 2: Regression coefficients and standard deviations of the inelastic GMPMs

Periods (s)	R_y=1.5	R_y=2	R_y=2.5	R_y=3	R_y=4	R_y=5	R_y=6	μ=1.5	μ =2	μ =2.5	μ =3	μ =4	μ =5	μ =6
0.1	-0.329	-0.395	-0.419	-0.429	-0.446	-0.452	-0.454	-0.342	-0.371	-0.385	-0.391	-0.404	-0.416	-0.424
0.15	-0.317	-0.381	-0.419	-0.441	-0.462	-0.47	-0.478	-0.368	-0.426	-0.444	-0.451	-0.456	-0.46	-0.462
0.2	-0.275	-0.338	-0.38	-0.401	-0.417	-0.426	-0.435	-0.287	-0.37	-0.381	-0.395	-0.408	-0.409	-0.416
0.3	-0.261	-0.311	-0.327	-0.341	-0.35	-0.349	-0.357	-0.266	-0.326	-0.347	-0.348	-0.338	-0.337	-0.337
0.5	-0.231	-0.313	-0.311	-0.291	-0.297	-0.301	-0.303	-0.26	-0.309	-0.332	-0.324	-0.311	-0.306	-0.302
0.75	-0.206	-0.289	-0.304	-0.3	-0.29	-0.3	-0.296	-0.228	-0.295	-0.338	-0.306	-0.301	-0.313	-0.3
1	-0.135	-0.176	-0.207	-0.228	-0.257	-0.262	-0.253	-0.14	-0.198	-0.239	-0.25	-0.252	-0.255	-0.251
1.5	-0.187	-0.222	-0.263	-0.271	-0.274	-0.277	-0.282	-0.216	-0.257	-0.28	-0.29	-0.299	-0.301	-0.291
2	-0.167	-0.219	-0.272	-0.301	-0.315	-0.322	-0.326	-0.193	-0.25	-0.278	-0.316	-0.34	-0.326	-0.308
3	-0.16	-0.231	-0.241	-0.253	-0.272	-0.287	-0.311	-0.198	-0.255	-0.264	-0.269	-0.275	-0.312	-0.338
4	-0.222	-0.265	-0.28	-0.309	-0.323	-0.337	-0.346	-0.253	-0.278	-0.299	-0.323	-0.347	-0.356	-0.342